Low latitude hydrogen emission at Jupiter

W. Kent Tobiska, Space Environment Technologies
Wayne R. Pryor, Space Environment Technologies
G. Randy Gladstone, Southwest Research Institute
Karen E. Simmons, Laboratory for Atmospheric and Space Physics

Scientific Objectives

Our study accomplished the first analysis of Galileo's low/mid latitude H Lyman-α data, which contains new information about the link between Jupiter's upper atmosphere, the magnetosphere, the dynamic lower atmosphere, and the Sun.

Background. Prior to the Galileo mission, Jupiter's hydrogen Lyman-α line at 121.57 nm was observed outside the auroral zones by a number of satellite instruments. The Pioneer 10 UV photometer first observed this emission in detail in 1973 [Judge and Carlson, 1974; Carlson and Judge, 1974; Judge *et al.,* 1976]. These observations were soon followed by the Voyager 1 and 2 ultraviolet spectrometers, which made a host of measurements as part of their objective of defining the upper atmosphere of Jupiter [Broadfoot *et al.,* 1981]. The Voyager 1 and 2 data were studied extensively [e.g., Broadfoot *et al.,* 1981; Sandel *et al.,* 1980; McConnell *et al.,* 1980] from the late 1970's into the 1980's at a time in which sounding rocket and IUE measurements continued to be made [e.g. Clarke *et al.,* 1980, 1981, 1982] during and after the Voyager encounters. The Hubble Space Telescope (HST) and the Hopkins Ultraviolet Telescope (HUT) made observations of Jupiter's upper atmosphere following launch but prior to arrival of Galileo.

On Jupiter, each look at non-auroral Lyman-α emission brought new questions regarding 1) the production mechanisms giving rise to the emission and 2) the energetic processes that give rise to inhomogeneities within Jupiter's upper atmosphere. Based on early estimates, for example, an average Lyman-α brightness of about 300 R was expected as the possible result of dissociative excitation of H_2. Carlson and Judge [1974] measured Lyman-α brightness of 400 R. Voyager I soon provided the first spatial maps of Lyman-α emission and Sandel *et al.* [1980] found significant north-south structure in the Voyager data including a longitudinally broad H bulge near 100° longitude. Dessler *et al.* [1981] suggested a link to the Jovian magnetosphere for this Lyman-α bulge and many observers confirmed that it was fixed in system III coordinates, i.e., that it rotates with the magnetosphere. McConnell *et al.* [1980] found a 700-1000 R longitudinal asymmetry on the darkside thus potentially eliminating a direct solar source. Skinner *et al.* [1988] noted short time variability in this emission. The source mechanism for maintaining this bulge is still not agreed upon. For example, Shemansky [1985] suggested charged particle collision as an energy deposition mechanism while Ben Jaffel *et al.* [1993] suggested turbulence in a non-thermal velocity field as a source of extra scattering opacity for reflecting solar Lyman-α.

On the dayside, resonant scattering of solar H Lyman-α photons by atmospheric hydrogen atoms is believed to be the dominant emission source. However, the solar photon scattering does not cause the longitudinal asymmetry near the bulge longitude. The solar Lyman-α irradiance is well known during the Galileo mission based on the UARS measurements at solar cycle minimum and is approximately $3.1 \pm 0.2 \times 10^{11}$ photons cm^{-2} s^{-1} at 1 AU. The small 27-day variation in this solar signal can be extracted from the resonantly scattered dayside Lyman-α emission on Jupiter. Work by Tobiska *et al.* [1997a] demonstrated that the Lyman-α variation is small.

The resonantly scattered photons from interplanetary hydrogen were measured by Galileo during the cruise to Jupiter and have been accurately modeled by Pryor *et al.* [1992, 1996]. The

solar variability within the interplanetary sky background emission that is seen by Jupiter's darkside can be removed from the Galileo Jupiter nightglow data by Pryor's model.

Galileo Prime Mission UVS data. The Galileo spacecraft was launched by the shuttle in October 1989 to study the Jovian system in detail with a complement of science instruments including an ultraviolet spectrometer (UVS) and an extreme ultraviolet spectrometer (EUV) [Hord *et al.,* 1992]. Galileo arrived at Jupiter on December 7, 1995 after an extensive voyage from Earth lasting six years. On-orbit, prime mission measurements by Galileo's UVS and EUV began in June 1996 and included targets of Jupiter's atmosphere and aurora. These measurements continue into the present with the Galileo Europa Mission (GEM). The prime mission (orbits G1-E11) Jupiter atmosphere observations by the UVS constitute a seminal dataset. Analysis of the auroral data has begun [Ajello *et al.,* 1998; Pryor *et al.,* 1998; James *et al.,* 1998] and the non-auroral data has been presented by Tobiska *et al.* [1997b, 1997c].

The extensive Galileo UVS Lyman-α measurements of low-latitude hydrogen have been made under a variety of geometry, temporal, and spatial conditions. These data provide the best measurement set compiled to-date to determine the source mechanism of the Lyman-α bulge, the magnetosphere/atmosphere coupling, and the possible dynamical energy exchange between the lower and upper atmosphere.

Study objectives. Resonant scattering of bright solar emission lines provides important diagnostics about the composition of many solar system objects, including Jupiter. The relevance of resonant scattering of bright solar lines to remote sensing of the planetary atmospheres has been reviewed by Meier [1991]. The backscatter of hydrogen Lyman-α line at 121.57 nm has been observed in the atmospheres of every planet in the solar system, from every comet observed, and from the interplanetary neutral gas. Knowledge of the solar Lyman-α flux is critical for understanding outer planet hydrocarbon photochemistry and aerosol formation. Lyman-a photolysis dissociates methane, forming radicals that react to form such disequilibrium chemicals as ethane and acetylene. Hydrogen densities inferred from solar-scattered Lyman-α brightness reveal structural and dynamical features in Jupiter's upper atmosphere.

One of the goals of the Galileo ultraviolet spectrometer team was to understand the spatial, temporal, and energetic interactions of Jupiter's upper atmosphere with its magnetosphere, the dynamical lower atmosphere, and with the Sun. Lyman-α was observable in mid and low latitude data collected by the UVS during its mission. Features that are clearly observable in the dataset and that are of particular interest include the hydrogen bulge, the spatial and local time distribution of hydrogen in the thermosphere, the temporal and dynamical variability of that hydrogen, and the nature of the extended corona. Study of the thermospheric hydrogen spatial distribution can answer *what accounts for observed longitudinal variations, what is the origin of variations on timescales from hours to months, and what physical processes generate these variations in hydrogen densities?*

Galileo UVS Lyman-α observations. A unique set of measurements of Jupiter's H Lyman-α brightness was obtained [Tobiska *et al.,* 1997b, 1997c; Ajello *et al.,* 1998] which covered all ten science orbits of the Galileo prime mission. Table 1-1 lists all of the Galileo UVS atmospheric and auroral observations in the prime mission while Table 1-2 lists all of the upper atmospheric non-auroral observations using Lyman-α as the main diagnostic wavelength. This is the most complete dataset of its kind, which includes darkside and brightside emissions obtained during low levels of solar flux (solar minimum) but with a variety of look directions into the sky background which glows with resonantly scattered Lyman-α.

Darkside Lyman-α. Darkside low latitude Lyman-α observations have been made at all longitudes by the Galileo UVS. There has been exceptionally good signal-to-noise ratio obtained in the observed counts (Figure 1) with an 88 grating step, 2 starting wavelength position com-

mand that has been used consistently during the prime mission. Not only are the data internally self-consistent (counts from both grating positions agreed with one another to within 11%), but the counts were also normalized using UARS solar flux to remove solar variability effects from sky background Lyman-α.

Table 1-1. Galileo UVS Atmospheric Objectives and Observations

Resolution / Objective	SYSTEM III (lat/lon)	HEMISPHERE (north-south/ day-night)	SHORT-TERM (≤ hours)	LONG-TERM (≥ weeks)
STRATOSPHERIC AEROSOLS and HYDROCARBONS				
Feature tracks:				
Great Red Spot & vortices	G1, C9			G1, C9
Acetylene distribution	G2			
belt-zone boundary	C3			
5 micron hot spot	E4			
white oval	E6			
brown barge	G7,E11			
southern polar haze	G8			
plume	C9			
hi phase crescent	C9			C9
northern polar haze	C10			
AURORAE				
EUV		G1, C3, E4, E6, G7, E11		G1, C3, E4, E6, G7, E11
(G) FUV	G1, G2, C3, G7, G8, C9, C10, E11	G1, G2, C3, E4, E6, G7, G8, C9, C10, E11	G1, C3, G7, G8, C9, C10, E11	G1, G2, C3, E4, E6, G7, G8, C9, C10, E11
(F) MUV	C3, G7, C9, C10, E11	G1, C3, E4, E6, G7, C9, C10, E11	C3, G7, C9, C10, E11	G1, C3, E4, E6, G7, C9, C10, E11
(N) NUV	C3, C10		C3, C10	
IMAGE/SPECTRA	C3, G7, C9, C10, E11		E11	
AIRGLOW				
Lyman-α distribution	G1, G2, C3, E4, E6, G7, G8, C9, C10, E11	G2, C10, E11	E4, G8	G1, G2, C3, E4, E6, G7, G8, C9, C10, E11
Lyman-α limb curve	G8, C10, E11	G1, G2, C10, E11		C10, E11
EUV H2 dayglow	G1, C3, E4, E6, E11	G1, C3, E4, E6, E11		G1, C3, E4, E6, E11
FUV H2 dayglow	E4, E6, G7, G8, C10, E11	G2, G8, C10, E11		E4, E6, G7, G8, C10, E11
Hydrogen corona	G8, C10, E11	C10, E11		C10, E11

Table 1-2. Galileo UVS Upper Atmospheric Airglow Observations by Orbit

Orbit	*Observation*	*UTC Start time*	*UTC End time*	*Lat/lon*	*Observation Objective*
G1A	G1JUFIXLON01	1996-175/23:43:31	1996-176/00:17:54	0/300-307	G/G Ly-a scan; equatorial zone hydrogen mapping; night
G1A	G1JUDRKMAP01	1996-176/00:50:15	1996-176/02:53:36	0/340-360 0/0-26	G/G Ly-a scan; equatorial zone hydrogen mapping; night
G2A	G2JUFIXLON01	1996-246/19:10:59	1996-247/00:18:22	0/80-100	G/G Ly-a scan; equatorial zone hydrogen mapping; night-day
G2A	G2JUDRKMAP01	1996-247/22:11:47	1996-247/23:46:50	0/275-310	G/G Ly-a scan; equatorial zone hydrogen mapping; night
G2A	G2JUBRTMAP01	1996-248/01:21:53	1996-248/06:29:15	+40/0-210 -40/0-210	G/G full scan; North-Eq-South global UV energy; day
G2A	G2JUNEWSMP01	1996-248/06:29:15	1996-248/07:10:43	+25/261-117 -25/261-117	F/G full scan; N-E-W-S map day-glow/electroglow; night-day
G2A	G2JUGLOMOS01	1996-249/01:05:31	1996-249/01:20:41	+60to-40/160-90	G/G Ly-a scan; global hydrogen mapping; day
C3A	C3JUFIXLON01	1996-308/19:53:29	1996-308/20:58:12	0/10-40	G/G Ly-a scan; equatorial zone hydrogen mapping; night
C3A	C3JUDRKMAP01	1996-308/20:58:12	1996-308/22:29:12	0/40-67	G/G Ly-a scan; equatorial zone hydrogen mapping; night
C3A	C3JUFIXLON02	1996-308/22:29:12	1996-309/01:31:12	0/120-206	G/G Ly-a scan; equatorial zone hydrogen mapping; night
C3A	C3JUDRKNEW01	1996-314/05:41:03	1996-314/06:53:51	-60/ 172-41 +60/ 172-41	F/G,N/G full scan; N-E-W-S map solar occultation; night
E4A	E4JUFIXTMB01	1996-350/16:04:33	1996-351/02:15:15	0/5-355	G/G full scan; Equatorial UV energy fixed local time; day
E4A	E4JUFIXLON01	1996-351/22:12:25	1996-352/03:19:47	0/90-310	G/G Ly-a scan; equatorial zone hydrogen mapping; night
E6A	E6JUDRKMAP01	1997-049/21:47:50	1997-050/00:53:53	0/346-60	G/G Ly-a scan; equatorial zone hydrogen mapping; night
E6A	E6JUFIXTMD01	1997-050/15:36:35	1997-050/18:42:37	0/277-359	G/G Ly-a scan; equatorial zone hydrogen mapping; night
G7A	G7JUDRKMAP01	1997-092/18:53:19	1997-092/20:28:22	0/225-280	G/G Ly-a scan; equatorial zone hydrogen mapping; night
G7A	G7JUFIXLON01	1997-093/05:56:37	1997-093/07:01:19	0/270-290	G/G Ly-a scan; equatorial zone hydrogen mapping; night
G8A	G8JUEWMAPS01	1997-126/14:33:27	1997-126/15:07:50	0/248-93	G/G Ly-a scan; equatorial zone and corona H map; night-day
G8A	G8JUDRKMAP01	1997-126/21:51:16	1997-126/23:26:18	0/65-101	G/G Ly-a scan; equatorial zone hydrogen mapping; night
G8A	G8JUFIXLON01	1997-127/06:08:44	1997-127/07:11:25	0/350-8	G/G Ly-a scan; equatorial zone hydrogen mapping; night
C9A	C9JUDRKMAP01	1997-177/03:40:16	1997-177/05:45:38	0/230-290	G/G Ly-a mini scan; equatorial zone hydrogen mapping; night
C10A	10JUDRKMAP01	1997-260/10:58:24	1997-260/12:33:26	0/30-70	G/G Ly-a mini scan; equatorial zone hydrogen mapping; night
C10A	10JUNEWSMP01	1997-260/12:33:26	1997-260/13:38:09	0/131-341	G/G Ly-a scan; equatorial zone and corona H map; night-day
C10A	10JUDRKMAP02	1997-260/19:01:42	1997-260/21:35:24	0/315	G/G Ly-a mini scan; equatorial zone hydrogen mapping; night
E11A	11JUDRKMAP01	1997-309/14:00:45	1997-309/16:06:07	0/320-18	G/G Ly-a mini scan; equatorial zone hydrogen mapping; night
E11A	11JUDRKMAP02	1997-309/18:58:01	1997-309/22:02:02	0/130-221	G/G Ly-a mini scan; equatorial zone hydrogen mapping; night
E11A	11JUEWMAPS01	1997-312/03:56:35	1997-312/04:28:56	0/90-250	G/G Ly-a scan; equatorial zone and corona H map; night-day

Figure 2 shows a system III map of equatorial H brightness for the darkside observations. A magnetically-coupled broad Lyman-α bulge is seen persisting since Voyagers 1 & 2, i.e., the bulge is fixed in System III. A cubic spline fit to the Galileo brightness yields a maximum at 82° longitude and a minimum at 304°. The fact that the longitude of maximum brightness is different from Voyager (82° vs 100°) [Broadfoot *et al.,* 1981; Sandel *et al.,* 1980] may be from Voyager sampling uncertainty. The intensity of the pre-dawn bulge ranges from 0.83–0.92 kR

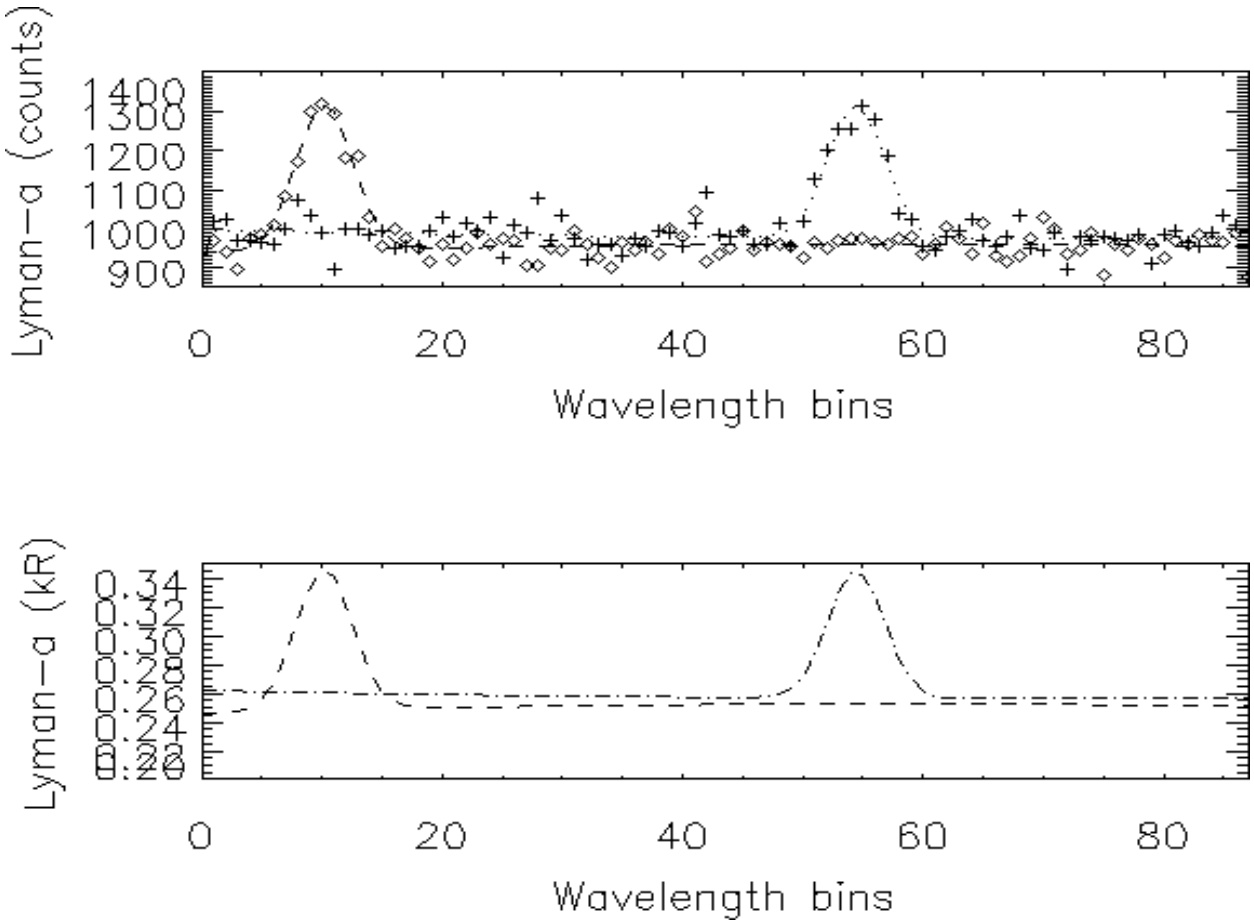

(SZA≈120°).

Figure 1. Typical darkside Lyman-α line profile shapes and background (units of counts) for two grating starting wavelength positions (top panel); Gaussian fit to line shape (units in kR) (bottom panel).

The Galileo bulge data are double the P10 400 R values and are in general agreement with later studies. They are also consistent with previously suggested production mechanisms, including magnetospherically related non-thermal velocity field (turbulent) heating from high velocity jets originating in the auroral zones [Ben Jaffel, *et al.* 1993; Sommeria *et al.* 1995; Emerich *et al.* 1996] or charged particle collision with thermospheric H [Shemansky, 1985; McGrath *et al.*, 1989; McGrath, 1991].

The Galileo UVS data may not have sufficient spectral resolution to distinguish between the two mechanisms but will potentially provide other evidence to answer the question *what is its origin, has it changed since the first observations by Voyagers 1 and 2, and what are the physical processes sustaining it?*

There also appear hydrogen enhancements and depletions that are localized, i.e., they are random in the System III reference frame. The variations range from 0.68 to 1.5 kR. These Galileo data validate previous observations of time or spatial variability and their variability suggests non-magnetosphere production mechanisms. The Galileo probe Atmosphere Structure Instrument (ASI) measured thermospheric temperatures and found wave-like phenomena at equatorial latitudes [Young *et. al.* 1997]. One explanation for enhanced H Lyman-α is increased or depleted density from heating/cooling due to viscous damping of gravity waves above the homopause.

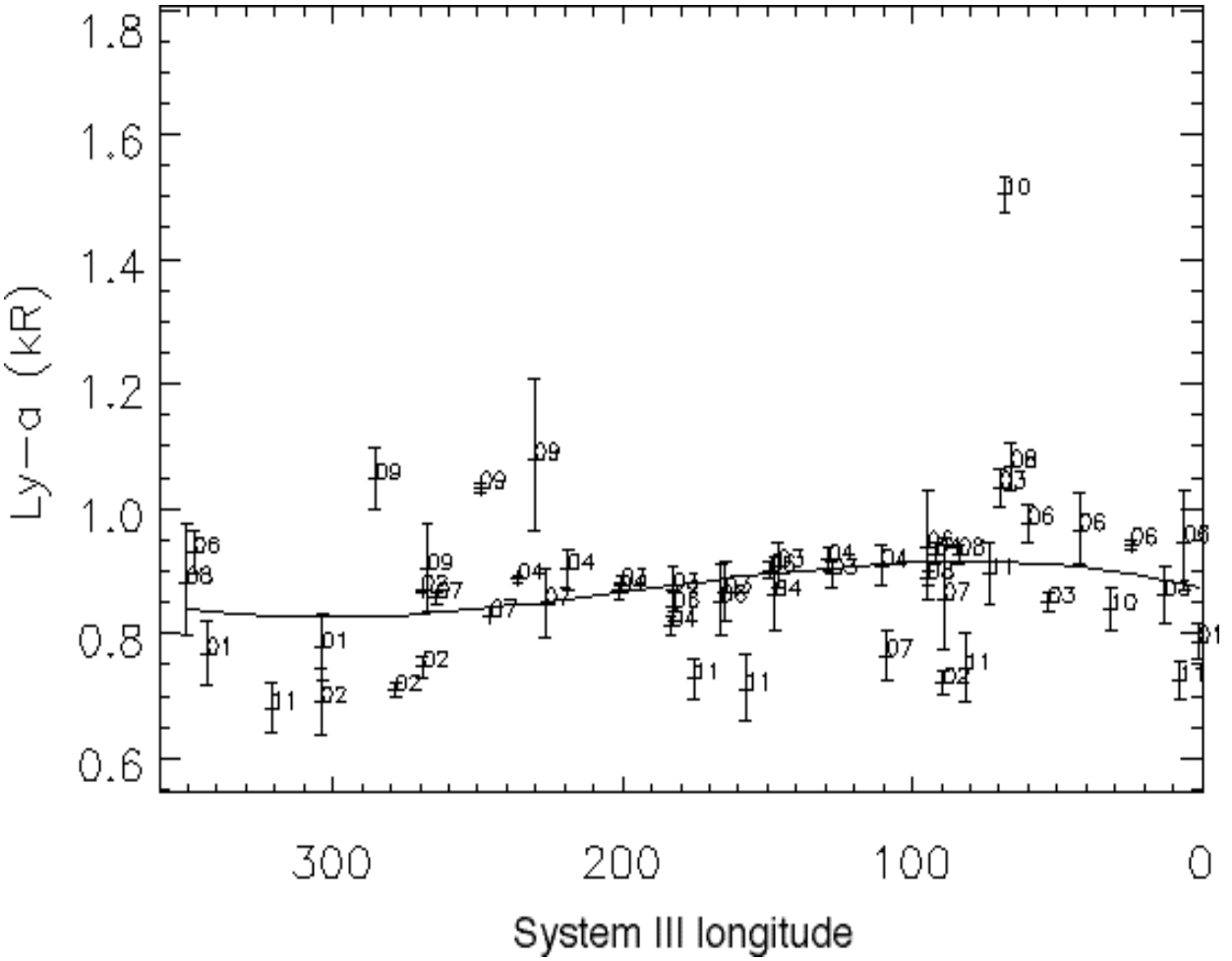

Figure 2. UVS darkside Lyman-α System III map from orbits G1-E11 shown as intensity (kR). Orbit numbers are also included along with the measurement uncertainty 1s error bars. The Lyman-α bulge maximum can be seen at 82° longitude.

Figure 3 shows a hint of lower atmospheric features dynamically perturbing thermospheric hydrogen. The data are replotted on a reference frame fixed with the Great Red Spot (GRS) in the center. The trailing vortices downstream of the GRS from Voyager 2 images extend to the left of center. The greatest variability in Lyman-α occurs in the regions surrounding the GRS. A subsequent study will evaluate the visible features (HST, IRTF, and Galileo SSI) under the UVS slit at the time of the observations to determine if the gravity wave mechanism associated with a unique feature is a feasible candidate for explaining the enhanced or depleted Lyman-α.

Dayside Lyman-α. The low-latitude dayside Lyman-α has been observed at a constant lighting (emission) angle for a full Jupiter rotation by the UVS. Additionally, high spatially-sampled

(recorded) datasets of the equatorial Lyman-α covering both midnight and noon limbs, the dawn terminator, and the hydrogen corona extending to more than 3 Rj have been obtained. Those data were analyzed with our radiative transfer model [Gladstone, 1988; Gladstone *et al.*, 2004] so as to understand the physical process observed.

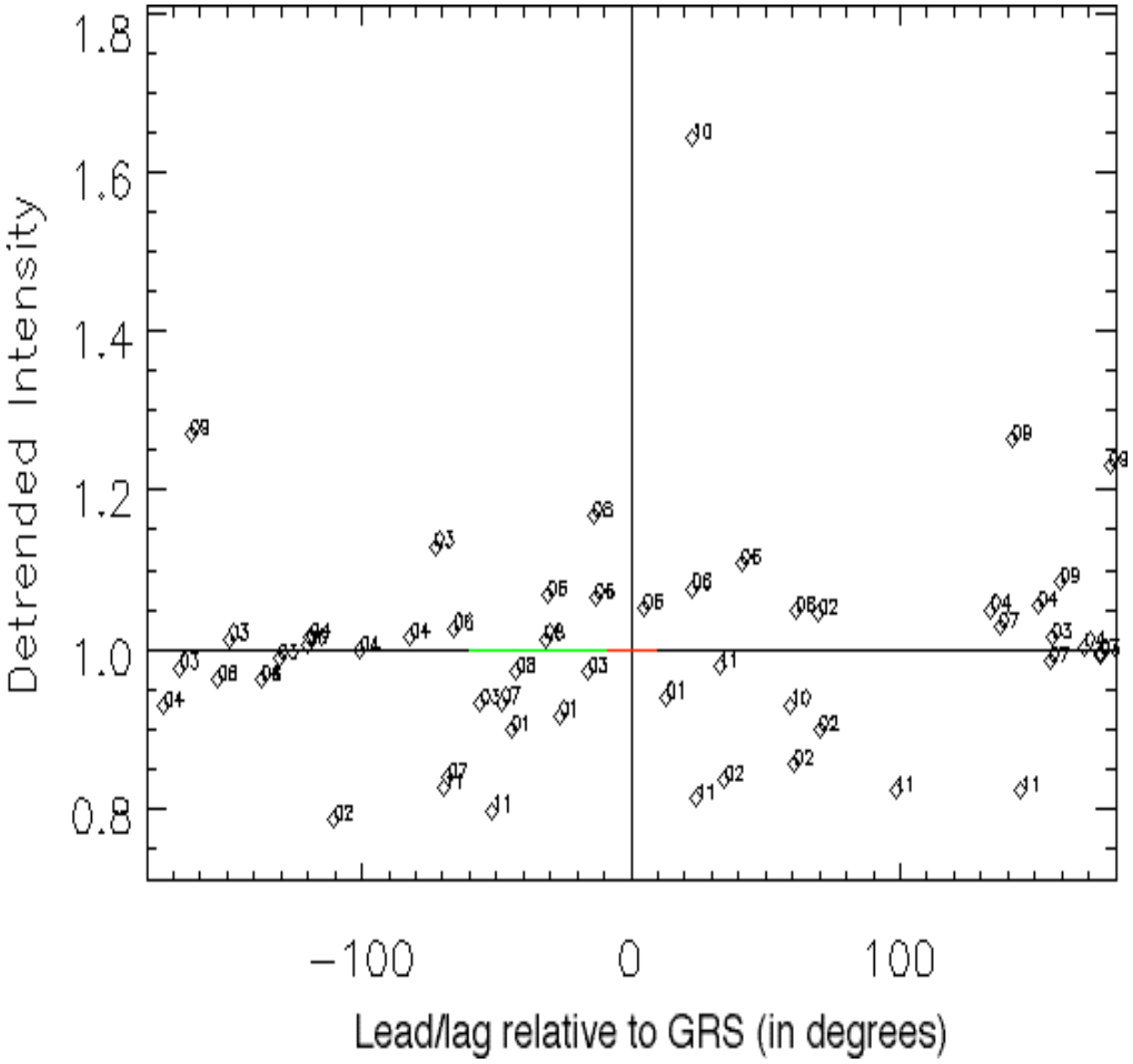

Figure 3. Enhanced and depleted Lyman-α emission (bulge detrended) can be seen in longitudes relative to the center of the GRS. The center bar (±10°) represents the longitudinal extent of the GRS; the gray bar (-10° to -60°) represents the extent of trailing vortices downstream of the GRS from Voyager 2 images. Greatest variability occurs in the regions surrounding the GRS.

An example of the quality of the dayside Lyman-α observations is the C10 "NEWS" map with northern (+30° latitude), equatorial, and southern (-30° latitude) swaths recorded for high (longitudinal) spatial structure. This observation, and a similar one in E11, also took extended measurements off the dark and bright limbs to beyond 3 Rj in the search of the hydrogen corona. Figure 4 shows the geometry of the observation in C10, Figure 5 shows the darkside/brightside

equatorial swath, and Figure 6 shows the expected brightness from a preliminary run of the radiative transfer model.

As for the hydrogen corona, we believe that the Galileo UVS data contain valuable insights into the extent, structure, and variability of that corona. Emerich *et al.* [1996] observed broad equatorial Lyman-α line profiles and we would expect an extended H corona in the sub-solar region, a feature not seen in the initial Galileo data (Figure 4). What the extent is of the corona, how does the hydrogen (either neutral or ionized) contribute to magnetospheric and other phenomena observed in the Jovian system, and what is the fate of the escaping hydrogen all still must be addressed more thoroughly.

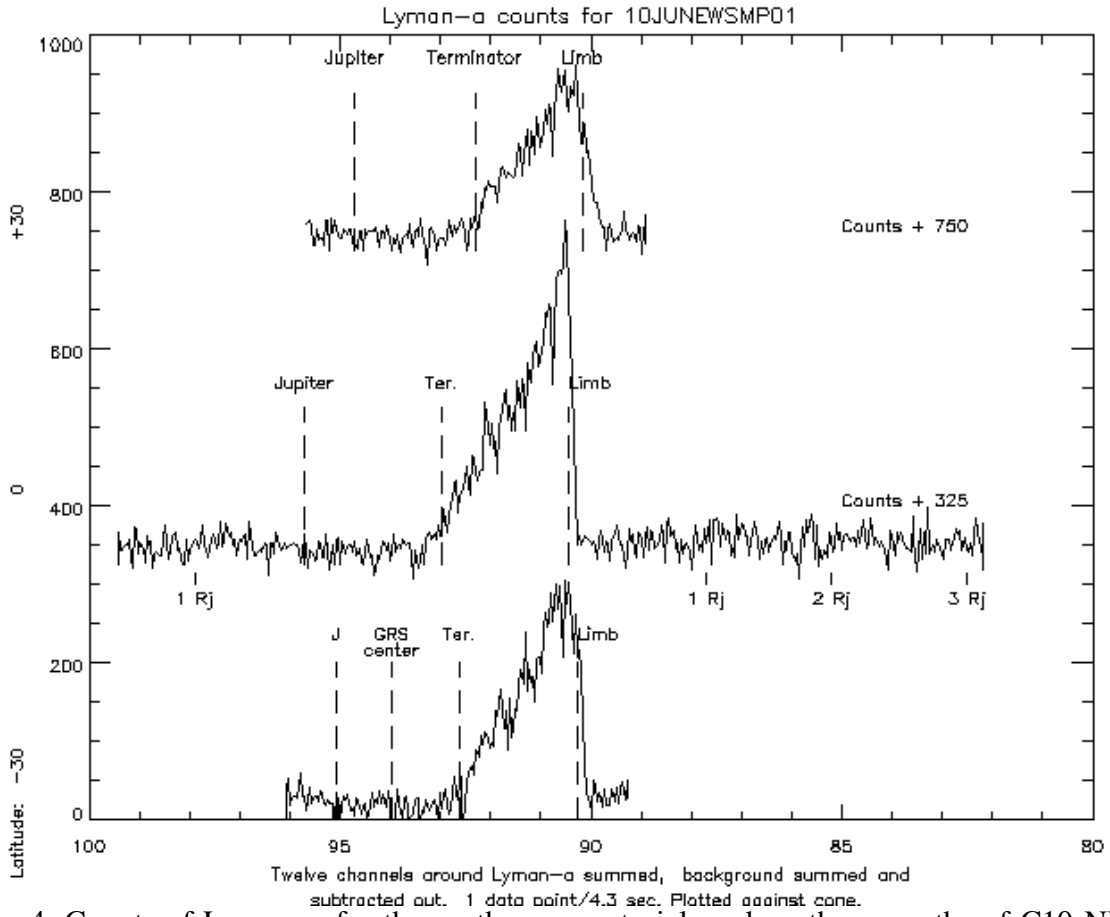

Figure 4. Counts of Lyman-α for the northern, equatorial, and southern swaths of C10 NEWS. Dark limb, terminator, and bright limbs are shown as is the GRS center on the darkside of the southern mid-latitude swath.

Organization of the data. The unanalyzed Galileo UVS Lyman-α observations from the prime mission for both dayside and nightside airglow (see Tables 1-1 and 1-2) were collected and sorted. We produced self-consistent, calibrated Lyman-α datasets in longitude, time, view angle, emission angle, and solar phase angle for archival in the PDS atmosphere node. These datasets provide the proper background of measurements against which we can model the Jovian airglow so as to understand the physical processes coupled to the magnetosphere, dynamical lower atmosphere, and the Sun that we are seeing.

The present state of knowledge on the Jovian hydrogen bulge, the hydrogen enhancements and depletions, and the corona have been summarized above. Further analysis of the Galileo

UVS data represents the next major step beyond Voyager, IUE, HUT, and HST for understanding the detailed energetic processes in Jupiter's upper atmosphere.

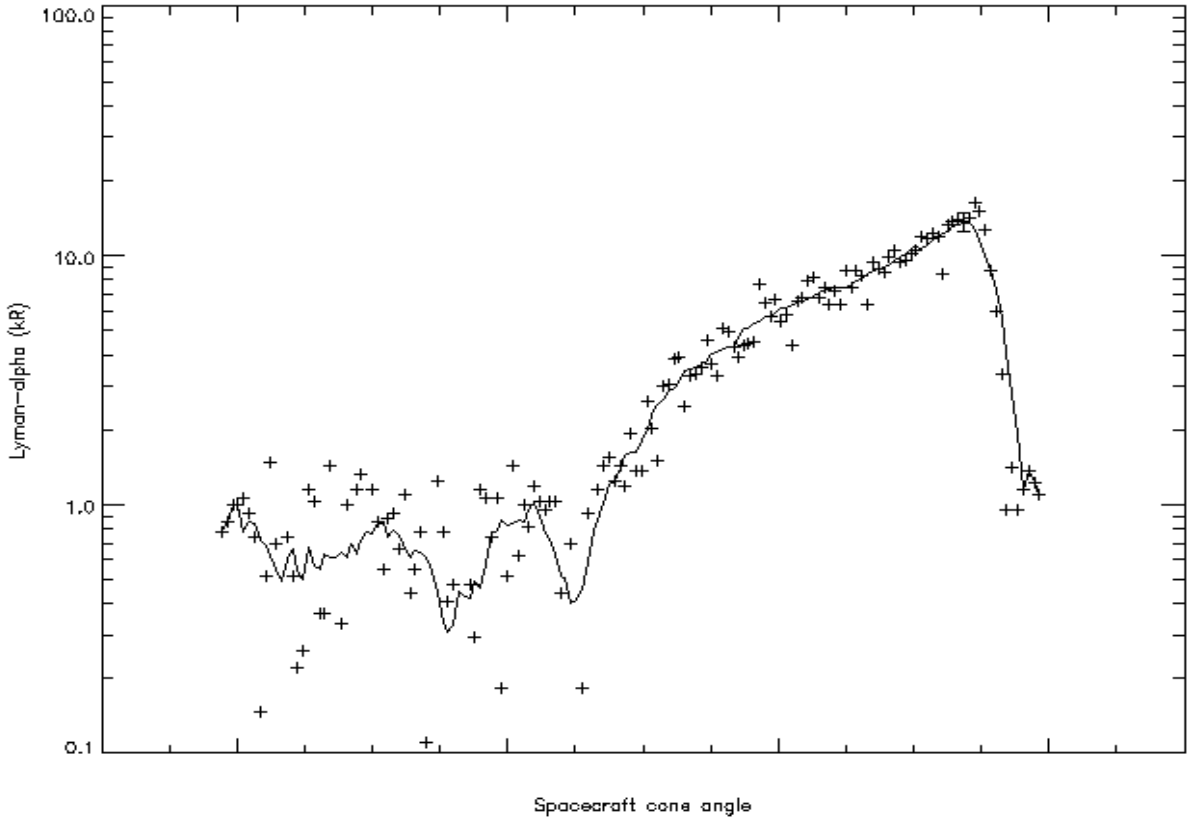

Figure 5. Galileo Lyman-α (in kR) for the equatorial swath on Jupiter during C10 NEWS. Peak intensity of ~2 times "normal H" in radiative transfer model (Figure 6) is consistent with previous results. Solar flux at 1 AU was 3.1×10^{11} photons cm^{-2} s^{-1} at 1 AU on 97-260 (solar minimum).

Data analysis and modeling methodology. Our data organization and analysis method was derived from IDL routines that have been developed by Tobiska for dataset first-looks and for data quality control during the prime mission. Our data is resident at the Laboratory for Atmospheric and Space Physics (LASP) at the University of Colorado and is accessible by a set of IDL routines developed by the UVS team at LASP. All raw science data and ancillary engineering data are available in data records organized by observation name, which were correlated with the experimenter's records at JPL. Throughout the prime mission, we developed a comprehensive workbook for each orbit's atmospheric observations, which constituted a 10-volume set. These team-published notes and the electronic data are available at LASP.

Several models were used in the course of our data analysis. Previous works by Tobiska and Pryor in solar and interplanetary Lyman-α variability are the basis for characterizing the exogenic radiation field that provides photons to the Jovian upper atmosphere.

Since the starting place for understanding Jupiter's Lyman-α emission is a knowledge of solar Lyman-α irradiance, we used the results of Tobiska *et al.* [1997a] as the solar signal for dayside airglow analysis. These solar Lyman-α data include the UARS SOLSTICE/SUSIM data during the Galileo period.

The model of Pryor *et al*. [1992, 1996] for knowledge of the interplanetary neutral gas distribution and the subsequent Lyman-α sky background in any particular look direction was used to understand the nightside resonantly scattered emission. Pryor, also a Co-I on the Galileo UVS, led the UVS team's Jupiter work in Colorado and collaborated closely with Tobiska in the design and analysis of Jupiter UVS data.

Gladstone [1988] developed a radiative transfer model appropriate for Lyman-α radiance and dayglow analysis of Jupiter's thermosphere. Using this model, we interpreted the Galileo measured brightness under different geometrical, spatial, and temporal steady state and perturbed conditions [Gladstone *et al.,* 2004]. For example, one area of interest is the characterization of the center-to-limb brightness curve and the expected sunlit limb brightness peak. Our observations of these features using Galileo should help to understand whether the low latitude H Lyman-α emission requires a substantial source of atomic hydrogen distributed across the planet or if there is an optically thin emitting process tied to the presence of sunlight. Figure 6 demonstrates, from Gladstone's radiative transfer model, the anticipated result for the Galileo UVS C10 NEWS observation.

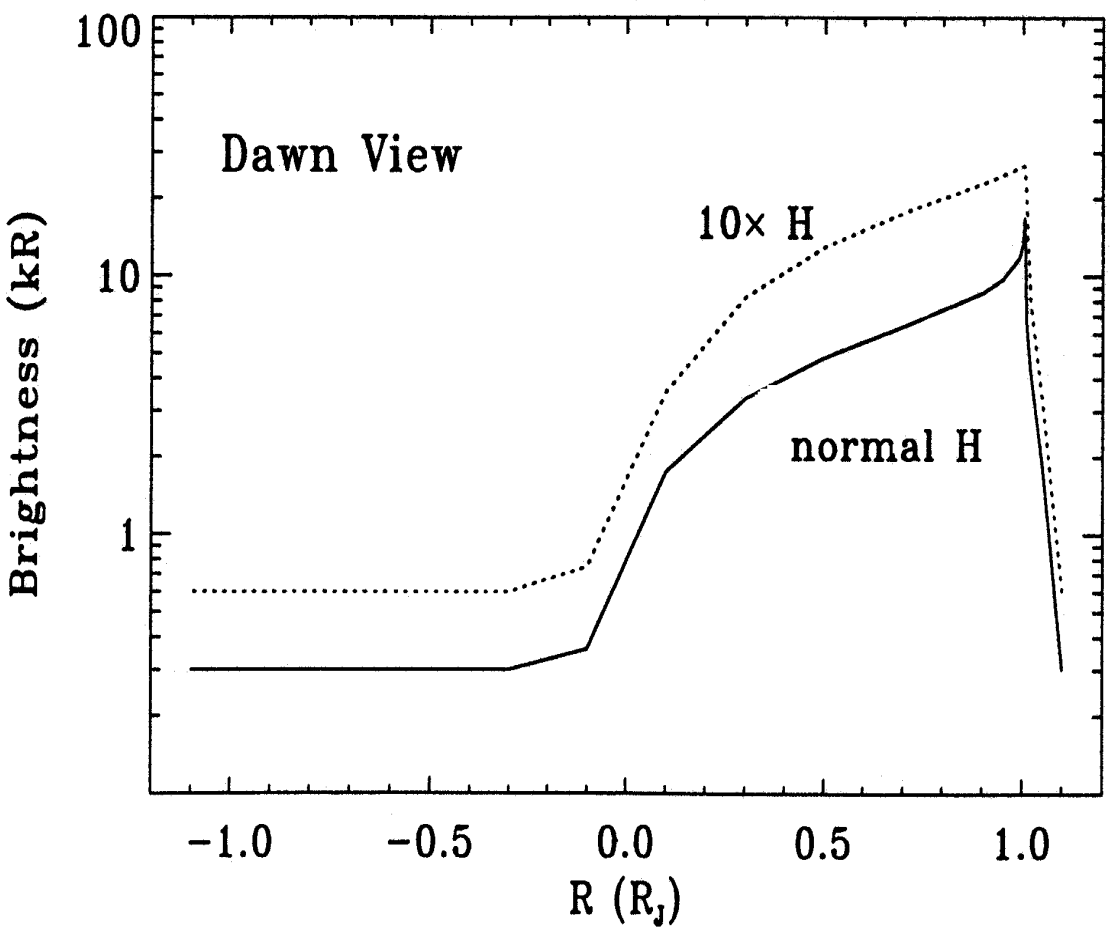

Figure 6. Radiative transfer model showing the expected Lyman-α brightness from Galileo's view above the (dawn terminator). The sharp spike for normal H column density (~1E17/cm3) is at the subsolar point. Estimated solar flux at 1 AU was 3.2E11.

Data product archival. We have archived in the PDS atmosphere node the following products: 1) the prime mission 10-volume comprehensive workbook for each orbit's UVS atmospheric observations and 2) the calibrated Lyman-α UVS datasets in longitude, time, view angle, emission angle, and solar phase angle. These data have been presented at annual scientific conferences.

Acknowledgements

NASA contract NASW-99022 provided funding for this work and is graciously acknowledged.

References

Ajello, J., *et al., J. Geophys. Res.,* accepted, (1998).
Ben Jaffel, L., *et al., Geophys. Res. Lett.,* **20,** 747, (1993).
Broadfoot, A.L., *et al., J. Geophys. Res.,* **86,** 8259, (1981).
Carlson, R.W. and D.L. Judge, *J. Geophys. Res.,* **79,** 3623, (1974).
Clarke, J.T., *et al., Astrophys. J.,* **240,** 696, (1980).
Clarke, J.T., *et al., Astrophys. J. Lett.,* **245**, L127, (1981).
Clarke, J.T., *et al., Astrophys. J.,* **255**, 806, (1982).
Dessler, A.J., *et al., Planet. Space Sci.,* **29,** 215, (1981).
Emerich, C., *et. al., Science,* **273**, 1085 (1996).
Gladstone, G.R., *J. Geophys. Res.,* **93,** 14623, (1988).
Gladstone, G. R., W. R. Pryor, W. K. Tobiska, W. K., A. I. F. Stewart, K. E. Simmons, and J. M. Ajello, *Planet. Space Sci.*, **52**, 415-421, 2004.
Hord, C., *et al., Space Sci. Rev.,* **60**, 503, (1992).
James, G. *et al., J. Geophys. Res.,* accepted, (1998).
Judge, D.L. and R.W. Carlson, *Science,* **183,** 317, (1974).
Judge, D.L., *et al.,* in *Jupiter,* T. Gehrel (Ed.), 1068, University of Arizona Press, (1976).
McConnell, J.C., *et al., Icarus,* **43,** 128, (1980).
McGrath, M., *et al., Geophys. Res. Lett.,* **16,** 583, (1989).
McGrath, M., *Geophys. Res. Lett.,* **18,** 1931, (1991).
Meier, R.R., *Space Sci. Rev.*, **58**, 1-186, (1991).
Pryor, W.R., *et al., Astrophys. J.,* **394**, 363, (1992).
Pryor, W.R., *et al., Geophys. Res. Lett.,* **23**, 1893, (1996).
Pryor, W.R., *et al., J. Geophys. Res.,* accepted, (1998).
Sandel, B.R., *et al*., *Geophys. Res. Lett.,* **7,** 5, (1980).
Shemansky, D.E., *J. Geophys. Res.,* **90,** 2673, (1985).
Skinner, T.E., *et al., J. Geophys. Res.,* **93,** 29, (1988).
Sommeria, J., *et. al., Icarus,* **119**, 2, (1995).
Tobiska, W.K., *et al., Geophys. Res. Lett.,* **24,** 1123, (1997a).
Tobiska, W.K., *et al., Geophys. Res. Lett.,* in preparation, (1997b).
Tobiska, W.K., *et al., EOS Suppl.,* **78**, S306, (1997c).
Young, L.A., *et. al., Science,* **276**, 108 (1997).